



Cite this: *Mater. Adv.*, 2021, 2, 3552Received 21st March 2021,
Accepted 11th May 2021

DOI: 10.1039/d1ma00243k

rsc.li/materials-advances

A nanoporous CeO₂ nanowire array by acid etching preparation: an efficient electrocatalyst for ambient N₂ reduction†

Yuyao Ji  and Xingquan Liu *

It is highly attractive but still remains a key challenge to develop earth-abundant electrocatalysts for efficient NH₃ electrosynthesis via the N₂ reduction reaction (NRR). In this work, a nanoporous CeO₂ nanowire array on a Ti mesh (np-CeO₂/TM) was derived from MnO₂-CeO₂/TM by acid etching of MnO₂ that acts as a pore-forming agent. In 0.1 M HCl, this catalyst achieves a high faradaic efficiency of 4.7% with a NH₃ yield of 38.6 μg h⁻¹ mg⁻¹_{cat.} at -0.3 V vs. reversible hydrogen electrode, outperforming most reported Ce-based NRR electrocatalysts under ambient conditions. It also demonstrates high electrochemical stability and excellent selectivity for NH₃ generation. The acid preparation strategy is highly valuable for future design of active NRR catalysts with desired compositions in various electrocatalysis fields.

As an important industrial chemical, NH₃ has attracted much attention as a potential energy carrier and a fertilizer precursor.^{1,2} With the increase of the population and the decrease of fossil fuels, the large demand for NH₃ has become an urgent social problem, which promotes the in-depth study of artificial NH₃ production technology. Due to the need for hydrogen input and energy consumption from fossil fuels, the traditional industry for producing ammonia (350–550 °C and 150–350 atm) is an energy intensive procedure: the Haber–Bosch process results in a great deal of carbon dioxide.³ Therefore, there is a tough impportunity for the development of facile and sustainable alternative strategies for NH₃ production.

As a kind of nitrogen reduction reaction (NRR) that can synthesize NH₃ at room temperature via using only a high efficiency electrocatalyst,^{4,5} the electrocatalytic NRR plays a significant role in attracting the attention of researchers.^{6–9} Recently, considerable attention has been focused on exploring non-noble-free NRR electrocatalysts.^{10–23} Porous noble metals are displayed to be effectual electrocatalysts for electrochemical storage and energy conversion,^{24–26} which need to be investigated

for the NRR. Instead of homogeneous metal surface, the coordinatively unsaturated active sites on phosphide surface might be beneficial for the bonding of nitrogen-related intermediates, is worth discussing in the NRR. Cerium(IV) oxide (CeO₂) has benefits of desirable electronic/ionic conductivity, and the cerium ion group plays a role as an intermediate in catalytic reaction and adsorption of gas, and is exposed.²⁷ Both element doping²⁸ and interface engineering²⁹ are verified productively to improve the NRR ability of catalysts. Porous nanostructures have the apparent advantage of high surface-area,³⁰ providing good benefit to improve the electrocatalytic NRR catalysis. It is thus trusted that constructing porous Ce-based catalysts is a good strategy to enhance the NRR activity of transition metal catalysts.

Herein, we report our finding that CeO₂ nanowires are a splendid catalyst for NH₃ synthesis under ambient conditions. The key idea is to selectively generate NP-CeO₂ nanowires with different corrosion stability, using oxalic acid on MnO₂ and CeO₂. CeO₂ achieves a high FE (4.7%) and NH₃ yield (38.6 μg h⁻¹ mg⁻¹_{cat.}) at -0.3 V vs. reversible hydrogen electrode (RHE), which are notably higher than those for the MnO₂-CeO₂ precursor (NH₃ yield: 14.3 μg h⁻¹ mg⁻¹_{cat.}, and FE: 1.6%) and most reported Ce-based NRR electrocatalysts under the conditions of 0.1 M HCl.

X-ray diffraction (XRD) results for CeO₂ (scratched down from TM) are shown in Fig. 1a. CeO₂ shows six peaks at 28.5°, 33.9°, 47.8°, 56.2°, 58.5°, and 69.1° indexed to the (111), (200), (220), (311), (222), and (400) facets of CeO₂ (JCPDS No. 43-1002), proposing the effective etching of MnO₂. As it is shown in the SEM image, MnO₂-CeO₂ nanowire arrays are anchored on TM (Fig. S1, ESI†), indicating that the construction of np-CeO₂/TM maintains the nanowire array feature (Fig. 1b). The transmission electron microscopy (TEM) image of etched np-CeO₂ is shown in Fig. 1e, which expresses a truth that the high-resolution TEM (HRTEM) supports interplanar distance of 0.313 nm corresponding to the (111) plane of CeO₂ (Fig. 1c).

The Brunauer–Emmett–Teller (BET) pore-size distribution curves of np-CeO₂ (Fig. 1e) exhibit an extensive peak centering at 8.6 nm, associated excellently with the TEM data. Meanwhile, the energy-dispersive X-ray (EDX) elemental mapping images of

School of Materials and Energy, University of Electronic Science and Technology of China, Chengdu 610054, China. E-mail: lxquan@uestc.edu.cn

† Electronic supplementary information (ESI) available. See DOI: 10.1039/d1ma00243k



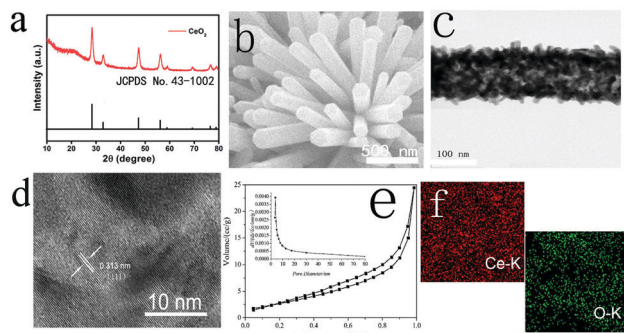


Fig. 1 (a) XRD patterns for np-CeO₂. SEM image of (b) np-CeO₂. TEM image of one single nanowire of (c) np-CeO₂. (d) HRTEM image of np-CeO₂. (e) Nitrogen adsorption/desorption isotherm plots and pore diameter of np-CeO₂. (f) EDX mapping images of CeO₂.

CeO₂ clearly show that Ce and O elements are evenly distributed on the surface. All these measurements absolutely prove the convincing formation of MnO₂-CeO₂ resulting in high surface area nanoporous CeO₂ nanowires under the condition of etching *via* acid.

X-ray photoelectron spectroscopy (XPS) was used to investigate the elemental composition and chemical valence states of porous CeO₂. As shown in Fig. 2b, high-resolution Ce 1s spectra (Fig. 2a) display binding energies of about 882.6 and 901.2 eV matching to Ce 3d_{5/2} and Ce 3d_{3/2}, accordingly.³¹ For O 1s, we can attribute it to three characteristic peaks. The two peaks at 530.1 and 531.7 eV correspond well to the ordered lattice oxygen ions of CeO₂, and the oxygen vacancy. For the peak at 533.3 eV, it can be defined to the absorbed hydroxyl on the surfaces of the CeO₂ from water molecules.^{32,33} The difference of peak area at 531.2 eV indicated that the oxygen vacancy of CeO₂ increased significantly during hydrogen reduction after acid treatment.^{34,35}

Conventional NRR is a conventional hydrogenation reduction after N₂ bubbling at the cathode surface, where H⁺ could convert the electrolyte to product NH₃ by reacting with CeO₂/N₂. For our experiment, the NRR tests were conducted in a two-chamber cell separately at ambient conditions, which is partitioned by a Nafion membrane (115). For our research, the NH₃ obtained at the cathode is formed by the interaction of N₂ and H⁺ by avoiding oxidation of the produced NH₃ at the anode, by avoiding passing through the spaced cell. At a moderate temperature and atmospheric pressure, the voltage was corrected by means of a reversible hydrogen electrode (RHE). The NH₃ and N₂H₄ produced by electrocatalytic reaction were determined *via* the indophenol blue

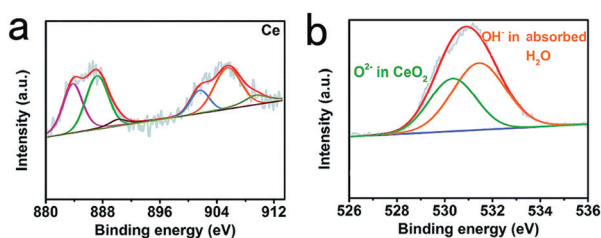


Fig. 2 XPS spectra of np-CeO₂ in the (a) Ce 3d and (b) O 1s regions.

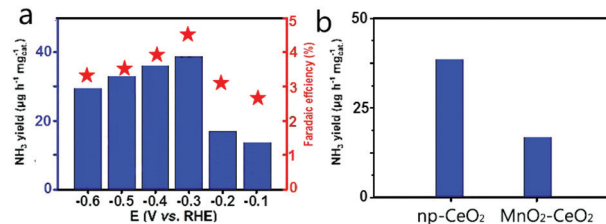


Fig. 3 (a) NH₃ yields and FEs at each given potential. (b) NH₃ yields with different catalysts at -0.3 V vs. RHE under ambient conditions.

method,³⁶ as well as by the Watt and Chrisp method.³⁷ The electrolyte was colored with indophenol indicator after 2 h electrocatalytic NRR reaction at constant potentials for collecting UV-Vis absorption spectra (Fig. S2 and S3, ESI[†]).

Np-CeO₂/GCE (0.3 mg cm⁻²) demonstrates exceptional selectivity without N₂H₄-production (Fig. S4, ESI[†]). Fig. 3b exhibits average NH₃ yields, and FEs at different potentials. In the study of the effect of load on catalytic activity, it was found that when the load was 0.3 mg, the best NRR activity was shown (Fig. S5, ESI[†]). The optimum NRR rate is fixed at -0.3 V vs. RHE, causing an average yield of 38.6 µg h⁻¹ mg⁻¹ cat. NH₃, and 4.7% FE. As a catalyst with good performance, it has a great advantage over most reported NRR catalysts, including Au nanorods (6.042 µg h⁻¹ mg⁻¹ cat., 4%),³⁸ Cu₃P-rGO (26.38 µg h⁻¹ mg⁻¹ cat., 1.9%),³⁹ γ-Fe₂O₃ (0.212 µg h⁻¹ mg⁻¹ cat., 1.9%),⁴⁰ and N-doped nanocarbon (27.2 µg L⁻¹ h⁻¹, 1.42%).⁴¹ Detailed comparison is presented in Table S1 (ESI[†]). Fig. 3a displays that the yield increases with the increase of potential. In view of the surface competitive adsorption between N₂ and H, the catalyst performance is significantly reduced when the voltage transcends -0.3 V. For comparison, we provide hydrogen yield rates for hydrogen evolution reactions (Fig. S5, ESI[†]). By comparing the pH test paper of the electrolyte solution before and after electrolysis (Fig. S6, ESI[†]), it can be concluded that the pH hardly changed in the experiment, which shows that the whole system has not transformed through the reaction. In Fig. 3b, np-CeO₂/GCE exhibits a speedier NRR rate than MnO₂-CeO₂/GCE (14.3 µg h⁻¹ mg⁻¹ cat.), demonstrating that the element N plays an important role in NRR. Meanwhile, in the whole process, the weak signal value expressed by the blank GCE is completely offset. To confirm that the sensed NH₃ is produced through NRR of np-CeO₂/GCE, a series of control experiments is conducted (experimental conditions: Ar for carrier gas, -0.3 V vs. RHE for open-circuit potential and 20 h for electrochemical reaction). Moreover, in 0.1 M HCl, we tested the NRR performance of the nanoporous CeO₂ nanowires deposited on carbon paper, and it also shows the greatest NH₃ yield of 34.6 µg h⁻¹ mg⁻¹ cat. and a high FE of 4.6% (Fig. S7, ESI[†]). For comparison purposes, the NH₃ yield and FE of the MnO₂-CeO₂ are shown in Fig. S8 (ESI[†]), and this result also demonstrates that np-CeO₂ has better NRR performance. Meanwhile, in 0.1 M H₂SO₄, our catalyst achieves a high FE of 4.61% along with a NH₃ yield of 36.9 µg h⁻¹ mg⁻¹ cat. at -0.3 V vs. RHE, and it shows almost no changes when measured in 0.1 M HCl and in 0.1 M H₂SO₄ (Fig. S9, ESI[†]).



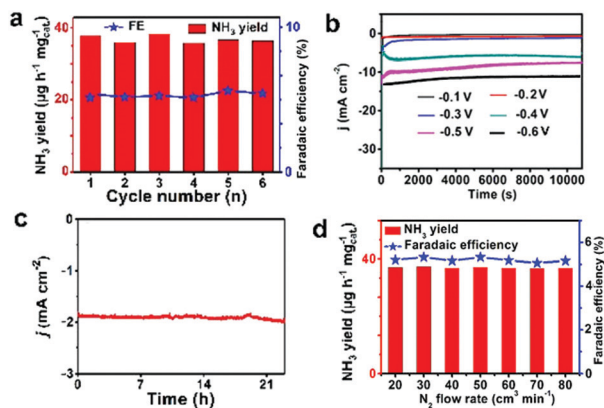


Fig. 4 (a) NH₃ yields and FEs at a potential of -0.3 V vs. RHE during recycling tests for 6 times. (b) Time-dependent current density curves for np-CeO₂ at different potentials. (c) Time-dependent current density curve for np-CeO₂ at -0.3 V vs. RHE. (d) NH₃ yields and FEs of the catalyst with different N₂ flow rates.

Stability is an additional significant parameter to estimate the catalyst behavior. np-CeO₂/TM has insignificant changes in NH₃ yield and FE through recycling experiments for 6 times (Fig. 4a). Fig. 4b displays the long-term electrolysis at a set of potentials, which indicates good stability of np-CeO₂/TM. Moreover, a slight change occurred after the NRR reaction at -0.3 V for 24 h (Fig. 4c). The XRD (Fig. S10, ESI[†]) and XPS (Fig. S11, ESI[†]) show almost no changes before and after the long test, and they also demonstrate high electrochemical stability. The FE for np-CeO₂ demonstrates slight loss compared to the initial one after long-term testing. Based on the experimental data, it can be concluded that np-CeO₂ is exceptionally stable and durable for the NRR under ambient reaction conditions. The influence of N₂ flow rate on electrocatalytic N₂ reduction was examined concurrently. What is shown in Fig. 4d is that there is inapparent fluctuation in FEs and NH₃ yields following a series of N₂ flow-rates, suggesting that the rate of reduction is impartial to the gas–solid interface. What is more, N₂ is transported toward the cathodic catalyst surface within the N₂ of the electrolyte. In addition, since the speed of electrocatalytic reaction is independent of N₂ concentration, it can be concluded that the diffusion of N₂ is not the decisive step of the reaction.

In summary, np-CeO₂ nanowire is proven as an efficient and selective electrocatalyst for NH₃ electrocatalysis from N₂ and water in acidic media. The np-CeO₂ nanowires attain a NH₃ yield of $38.6 \mu\text{g h}^{-1} \text{mg}^{-1}_{\text{cat}}$ and an FE of 4.7% at a potential of -0.3 V. Besides, what is surprising is that np-CeO₂ possesses appealing selectivity and long-term stability for electro-hydrogenation under ambient conditions. This investigation is not only the first demonstration of applying np-CeO₂ for efficient and stable NRR electrocatalysis, but would expose a stimulating new path to the advancement of transition metal nitrides as attractive low-cost NRR catalyst materials for implementations.

Conflicts of interest

There are no conflicts to declare.

Acknowledgements

This work was supported by the National Natural Science Foundation of China (No. 21575050).

Notes and references

- R. Schlögl, Catalytic synthesis of ammonia—a “never-ending story”?, *Angew. Chem., Int. Ed.*, 2003, **42**, 2004–2008.
- W. Gu, Y. Guo, Q. Li, Y. Tian and K. Chu, Lithium iron oxide (LiFeO₂) for electroreduction of dinitrogen to ammonia, *ACS Appl. Mater. Interfaces*, 2020, **12**, 37258–37264.
- I. Dybkjaer, In *Ammonia: catalysis and manufacture*, ed. A. Nielsen, Springer, Heidelberg, 1995, 199–308.
- S. Li, Y. Wang, J. Liang, T. Xu, D. Ma, Q. Liu, T. Li, S. Xu, G. Chen, A. M. Asiri, Y. Luo, Q. Wu and X. Sun, TiB₂ thin film enabled efficient NH₃ electrocatalysis at ambient conditions, *Mater. Today Phys.*, 2021, **18**, 100396.
- S. Gao, Y. Zhu, Y. Chen, M. Tian, Y. Yang, T. Jiang and Z. Wang, Self-power electroreduction of N₂ into NH₃ by 3D printed triboelectric nanogenerators, *Mater. Today*, 2019, **28**, 17–24.
- Y. Ji, L. Li, W. Cheng, Y. Xiao, C. Li and X. Liu, A CeP nanoparticle-reduced graphene oxide hybrid: an efficient electrocatalyst for the NH₃ synthesis under ambient conditions., *Inorg. Chem. Front.*, 2021, **8**, 2103–2106.
- T. Xu, B. Ma, J. Liang, L. Yue, Q. Liu, T. Li, H. Zhao, Y. Luo, S. Lu and X. Sun, Recent progress in metal-free electrocatalysts toward ambient N₂ reduction reaction., *Acta Phys.-Chim. Sin.*, 2021, **37**, 2009043.
- J. Wang, L. Yu, L. Hu, G. Chen, H. Xin and X. Feng, Ambient ammonia synthesis via palladium-catalyzed electro hydrogenation of dinitrogen at low overpotential, *Nat. Commun.*, 2018, **9**, 1795.
- K. Chu, Y. Liu, Y. Li, Y. Guo and Y. Tian, Two-dimensional (2D)/2D interface engineering of a MoS₂/C₃N₄ heterostructure for promoted electrocatalytic nitrogen fixation, *ACS Appl. Mater. Interfaces*, 2020, **12**, 7081–7090.
- S. Chen, S. Perathoner, C. Ampelli, C. Mebrahtu, D. Su and G. Centi, Electrocatalytic synthesis of ammonia at room temperature and atmospheric pressure from water and nitrogen on a carbon-nanotube-based electrocatalyst, *Angew. Chem., Int. Ed.*, 2017, **56**, 2699–2703.
- T. Wang, S. Li, B. He, X. Zhu, Y. Luo, Q. Liu, T. Li, S. Lu, C. Ye, A. M. Asiri and X. Sun, Commercial indium-tin oxide glass: a catalyst electrode for efficient N₂ reduction at ambient conditions, *Chin. J. Catal.*, 2021, **42**, 1024–1029.
- C. Li, D. Ma, S. Mou, Y. Luo, B. Ma, S. Lu, G. Cui, Q. Li, Q. Liu and X. Sun, Porous LaFeO₃ nanofiber with oxygen vacancies as an efficient electrocatalyst for N₂ conversion to NH₃ under ambient conditions, *J. Energy Chem.*, 2020, **50**, 402–408.
- C. Lv, Y. Qian, C. Yan, Y. Ding, Y. Liu, G. Chen and G. Yu, Defect engineering metal-free polymeric carbon nitride electrocatalyst for effective nitrogen fixation under ambient conditions, *Angew. Chem., Int. Ed.*, 2018, **57**, 10246–10250.
- B. Ma, J. Liang, T. Li, Q. Liu, Y. Luo, S. Lu, A. M. Asiri, D. Ma and X. Sun, Iron-group electrocatalysts for ambient nitrogen



- reduction reaction in aqueous media, *Nano Res.*, 2021, **14**, 555–569.
- 15 S. Mukherjee, D. A. Cullen, S. Karakalos, K. Liu, H. Zhang, S. Zhao, H. Xu, K. L. More, G. Wang and G. Wu, Metal-organic framework-derived nitrogen-doped highly disordered carbon for electrochemical ammonia synthesis using N₂ and H₂O in alkaline electrolytes, *Nano Energy*, 2018, **48**, 217–226.
 - 16 T. Wang, Q. Liu, T. Li, S. Lu, G. Chen, X. Shi, A. M. Asiri, Y. Luo, D. Ma and X. Sun, Magnetron sputtered Mo₃Si thin film: an efficient electrocatalyst for N₂ reduction at ambient conditions, *J. Mater. Chem. A*, 2021, **9**, 884–888.
 - 17 Y. Liu, M. Han, Q. Xiong, S. Zhang, C. Zhao, W. Gong, G. Wang, H. Zhang and H. Zhao, Dramatically enhanced ambient ammonia electrosynthesis performance by in-operando created Li-S interactions on MoS₂ electrocatalyst, *Adv. Energy Mater.*, 2019, **9**, 1803935.
 - 18 Q. Li, Y. Guo, Y. Tian, W. Liu and K. Chu, Activating VS₂ basal planes for enhanced NRR electrocatalysis: the synergistic role of S-vacancies and B dopants, *J. Mater. Chem. A*, 2020, **8**, 16195–16202.
 - 19 K. Chu, J. Wang, Y. Liu, Q. Li and Y. Guo, Mo-doped SnS₂ with enriched S-vacancies for highly efficient electrocatalytic N₂ reduction: the critical role of the Mo–Sn–Sn trimer, *J. Mater. Chem. A*, 2020, **8**, 7117–7124.
 - 20 H. Jin, L. Li, X. Liu, C. Tang, W. Xu, S. Chen, L. Song, Y. Zheng and S. Qiao, Nitrogen vacancies on 2D layered W₂N₃: a stable and efficient active site for nitrogen reduction reaction., *Adv. Mater.*, 2019, **31**, 1902709.
 - 21 H. Cheng, L. Ding, G. Chen, L. Zhang, J. Xue and H. Wang, Nitrogen reduction reaction: molybdenum carbide nanodots enable efficient electrocatalytic nitrogen fixation under ambient condition, *Adv. Mater.*, 2018, **30**, 1803694.
 - 22 P. Wei, Q. Geng, A. I. Channa, X. Tong, Y. Luo, S. Lu, G. Chen, S. Gao, Z. Wang and X. Sun, Electrocatalytic N₂ reduction to NH₃ with high faradaic efficiency enabled by vanadium phosphide nanoparticle on V foil, *Nano Res.*, 2020, **13**, 2967–2972.
 - 23 F. Wang, X. Lv, X. Zhu, J. Du, S. Lu, A. A. Alshehri, K. A. Alzahrani, B. Zheng and X. Sun, Bi nanodendrites for efficient electrocatalytic N₂ fixation to NH₃ under ambient conditions, *Chem. Commun.*, 2020, **56**, 2107–2110.
 - 24 O. D. Velev, P. M. Tessier, A. M. Lenhoff and E. W. Kaler, Materials: a class of porous metallic nanostructures, *Nature*, 1999, **401**, 548.
 - 25 M. Chen, Y. Zhang, L. Xing, Y. Qiu, S. Yang and W. Li, Nanopores: activatable photoacoustic nanopores for in vivo ratio-metric imaging of peroxynitrite, *Adv. Mater.*, 2017, **29**, 1607015.
 - 26 V. Malgras, H. Atae-Esfahani, H. Wang, B. Jiang, C. Li, K. C. W. Wu, J. H. Kim and Y. Yamauchi, ChemInform abstract: nanoarchitectures for mesoporous metals, *Adv. Mater.*, 2016, **28**, 993–1010.
 - 27 Y. Ji, J. Liu, S. Hao, Y. Xiao, L. Li and X. Liu, Full water splitting by a nanoporous CeO₂ nanowire array under alkaline conditions, *Inorg. Chem. Front.*, 2020, **7**, 2533–2537.
 - 28 T. Wu, X. Li, X. Zhu, S. Mou, Y. Luo, X. Shi, A. M. Asiri, Y. Zhang, B. Zheng, H. Zhao and X. Sun, P-doped graphene toward enhanced electrocatalytic N₂ reduction, *Chem. Commun.*, 2020, **56**, 1831–1834.
 - 29 W. Guo, Z. Liang, J. Zhao, B. Zhu, K. Cai, R. Zou and Q. Xu, Recent advances in graphene quantum dots: synthesis, properties, and applications, *Small Methods*, 2018, **2**, 1800204.
 - 30 X. Zhu, S. Mou, Q. Peng, Q. Liu, Y. Luo, G. Chen, S. Gao and X. Sun, Aqueous electrocatalytic N₂ reduction for ambient NH₃ synthesis: recent advances in catalysts developing and performances boosting, *J. Mater. Chem. A*, 2020, **8**, 1545–1556.
 - 31 K. Chu, Y. Cheng, Q. Li, Y. Liu and Y. Tian, Fe-doping induced morphological changes oxygen vacancies and Ce³⁺–Ce³⁺ pairs in CeO₂ for promoting electrocatalytic nitrogen fixation, *J. Mater. Chem. A*, 2020, **8**, 5865–5873.
 - 32 K. Chu, Q. Li, Y. Cheng and Y. Liu, Efficient electrocatalytic nitrogen fixation on FeMoO₄ nanorods, *ACS Appl. Mater. Interfaces*, 2020, **12**, 11789–11796.
 - 33 K. Chu, Y. Liu, Y. Cheng and Q. Li, Synergistic boron-dopants and boron-induced oxygen vacancies in MnO₂ nanosheets to promote electrocatalytic nitrogen reduction, *J. Mater. Chem. A*, 2020, **8**, 5200–5208.
 - 34 G. Zhu, J. Zhu, W. Jiang, Z. Zhang, J. Wang, Y. Zhuang and Q. Zhang, Semimetallic MoP₂: an active and stable hydrogen evolution electrocatalyst over the whole pH range, *Nanoscale*, 2016, **8**, 8500–8504.
 - 35 Z. Geng, X. Kong, W. Chen, H. Su, Y. Liu, F. Cai, G. Wang and J. Zeng, Oxygen vacancies in ZnO nanosheets enhance CO₂ electrochemical reduction to CO, *Angew. Chem., Int. Ed.*, 2018, **57**, 6054–6059.
 - 36 D. Zhu, L. Zhang, R. E. Ruther and R. J. Hamers, Photo-illuminated diamond as a solid-state source of solvated electrons in water for nitrogen reduction, *Nat. Mater.*, 2013, **12**, 836–841.
 - 37 G. W. Watt and J. D. Chrisp, Photoinactivation and carbethoxylation of leucine aminopeptidase, *Anal. Chem.*, 2012, **24**, 2006–2008.
 - 38 D. Bao, Q. Zhang, F. Meng, H. Zhong, M. Shi, Y. Zhang, J. Yan, Q. Jiang and X. Zhang, Electrochemical reduction of N₂ under ambient conditions for artificial N₂ fixation and renewable energy storage using N₂/NH₃ cycle, *Adv. Mater.*, 2017, **29**, 1604799.
 - 39 R. Zhao, Q. Geng, L. Chang, P. Wei, Y. Luo, X. Shi, A. M. Asiri, S. Lu, Z. Wang and X. Sun, Cu₃P nanoparticles-reduced graphene oxide hybrid: an efficient electrocatalyst to realize N₂-to-NH₃ conversion under ambient conditions, *Chem. Commun.*, 2020, **56**, 9328–9331.
 - 40 J. Kong, A. Lim, C. Yoon, J. H. Jang, H. C. Ham, J. Han, S. Nam, D. Kim, Y.-E. Sung, J. Choi and H. S. Park, Electrochemical synthesis of NH₃ at low temperature and atmospheric pressure using a γ-Fe₂O₃ catalyst, *ACS Sustainable Chem. Eng.*, 2017, **5**, 10986–10995.
 - 41 Y. Liu, Y. Su, X. Quan, X. Fan, S. Chen, H. Yu, H. Zhao, Y. Zhang and J. Zhao, Facile ammonia synthesis from electrocatalytic N₂ reduction under ambient conditions on N-doped porous carbon, *ACS Catal.*, 2018, **8**, 1186–1191.

